CHEMISTRY
A European Journal

A Journal of
ChemPubSoc Europe

Accepted Article

Title: A Ru(II) Polypyridyl Alkyne Complex Based Metal−Organic Frameworks for Combined Photodynamic/Photothermal/Chemo-Therapy

Authors: Xiaochun Hu, Yonglin Lu, Chunyan Dong, Wenrong Zhao, Xuewen Wu, Lulu Zhou, Lv Chen, Tianming Yao, and Shuo Shi

To be cited as: *Chem. Eur. J.* 10.1002/chem.201904704

Link to VoR: http://dx.doi.org/10.1002/chem.201904704

Supported by
ACES

WILEY-VCH

10.1002/chem.201904704

WILEY-VCH

FULL PAPER

A Ru(II) Polypyridyl Alkyne Complex Based Metal−Organic Frameworks for Combined Photodynamic/Photothermal/Chemo-Therapy

Xiaochun Hu [ab], Yonglin Lu [b], Chunyan Dong [b], Wenrong Zhao [b], Xuewen Wu [a], Lulu Zhou [a], Lv Chen [b], Tianming Yao *[a], Shuo Shi*[ab]

Abstract: Despite drug delivery nanoplatforms have received extensive attention, development of a simple, effective and multifunctional theranostics nanoplatform still remains a challenge. Herein, a versatile nanoplatform based on zirconium-framework (UiO-66-N_3) was synthesized, which demonstrated a combined photodynamic therapy (PDT), phothothermal therapy (PTT) and chemotherapy (CT) for cancer treatment. A Ru(II) polypyridyl alkyne complex (Ra) as a photosensitizer was modified into nanoplatform by click reaction for the first time. When exposed to applicable light irradiation, the as-prepared multifunctional nanoplatform (UiO-Ra-DOX-CuS) not only demonstrated an efficient $^1O_2$ generation, but also exhibited excellent photothermal conversion ability. In particular, the nanotherapeutic agent existed dual-stimuli response, either acidic environment or NIR laser irradiation would trigger the drug release. The synergetic efficacy of UiO-Ra-DOX-CuS combined PDT, PTT and CT was evaluated by cell experiments. Moreover, the design would promote the development of Ru(II) polypyridyl alkyne complexes based multifunctional nanoparticles and multimodal cancer treatment.

Introduction

Currently, chemotherapy (CT) is one of the most used strategies for cancer treatment.[1] However, the emergence of chemo-resistance and severe side effects limit its long-term curative efficacy. To address these problems and improve the therapeutic efficacy of CT, the combination of photothermal therapy (PTT), photodynamic therapy (PDT) and CT for advanced synergistic therapy has drawn much attention.[2]

PTT, converting light energy into thermal energy, would not only kill cancer cells by hyperthermia, but also may induce the release of the drug in the tumor area,[2a, 3] thereby enhancing the cancer therapy by synergistic treatment. During the past few decades, many kinds of nanomaterials with good photothermal conversion ability have been explored as PTT agents, such as graphene oxide,[4] Fe-based nanomaterials,[5] polydopamine NPs[6] and gold-based NPs.[7] Currently, CuS NPs, a kind of chalcogenide semiconductor nanoparticles, have been developed as a common PTT agent. The advantage of CuS NPs is that they have a broad absorption band (700-1100 nm),[2a, 8] which has an ideal overlap with NIR biological window.

[a] Shanghai Key Lab of Chemical Assessment and Sustainability, School of Chemical Science and Engineering, Tongji University, 1239 Siping Road, Shanghai 200092, P.R. China.
E-mail: tmyao@tongji.edu.cn, shishuo@tongji.edu.cn
[b] Breast Cancer Center, Shanghai East Hospital, Tongji University, Shanghai 200120, P.R. China

PDT is an oxygen-mediated minimally invasive therapeutic modality and the principle of PDT starts with the activation of a photosensitizer with harmless visible light.[4] Ru(II) complexes, especially Ru(II) polypyridyl complexes, are promising photosensitizers (PSs) in PDT applications due to their high thermal, chemical and photochemical stabilities, and high quantum yields.[9] Furthermore, their functional groups are adjustable and structures can be easily modified. However, poor water solubility, weak resistance to aggregation and low selectivity towards tumor of Ru(II) polypyridyl complexes limit their PDT applications as PSs. In recent years, to overcome these problems, many works based on the absorption or conjugation of Ru(II) polypyridyl complexes with nanoparticles have been published.[10] Among them, metal organic frameworks (MOFs) nanocarrier-based nanoplatform has been developed rapidly, because of their high surface area, substantial pore structure and alterable ligands, which would produce therapeutic treatment through loading agents by multiple methods.[2a, 11] In the meantime, the click reaction with high yield under mild conditions has become a powerful tool in the fabrication and bioconjugation of a lot of MOFs for the anti-cancer treatment and drug delivery.[12] To the best of our knowledge, there is no example of MOFs modified with Ru(II) polypyridyl complexes by click reaction, and the research that Ru(II) polypyridyl complexes and PTT agents as well as anti-cancer drugs were integrated into one platform is also scarce.

In this work, a newly multi-functionalized nanoplatform named UiO-Ra-DOX-CuS was synthesized. A Ru(II) polypyridyl alkyne complex as a photosensitizer was modified into MOFs by click reaction for the first time, and during the constructing, DOX was incorporated into porous of MOFs to play a role of chemotherapy, and small CuS NPs as a PTT agent was loaded on the surface of nanoplatform by physical absorption. In our approach, UiO-Ra-DOX-CuS NPs can generate $^1O_2$ efficiently and exhibit excellent photothermal conversion ability simultaneously. Meanwhile, the progress of DOX releasing can be promoted by either acid condition or photothermal reaction. In addition, our designed nanoplatform with a diameter about 110 nm was beneficial to enhanced permeability and retention (EPR) effect.[13] Our multifunctional nanoplatform provides a new approach that the utilization of Ru(II) polypyridyl alkyne complexes for nanoparticles mediated PDT, PTT and CT synergistic treatment.

Results and Discussion

Initially, a photosensitizer, based on a ruthenium(II) complex having an alkynyl group in its main ligand (Ra) (Scheme 1(a)), was synthesized and characterized as our previous work[14]. The

weak changes in UV-Vis spectroscopy over time indicated that Ra was stable in aqueous and PBS (pH=7.4) solution (Figure S1). And then, to realize our multifunctional nanoplatform, UiO-66-N_3 with a narrow size distribution (Figure S2) was synthesized. Scanning electron microscopy (SEM) and transmission electron microscopy (TEM) images (Figure 1A) of the light-yellow product revealed that the nanoparticles have an average diameter of about 110 nm.

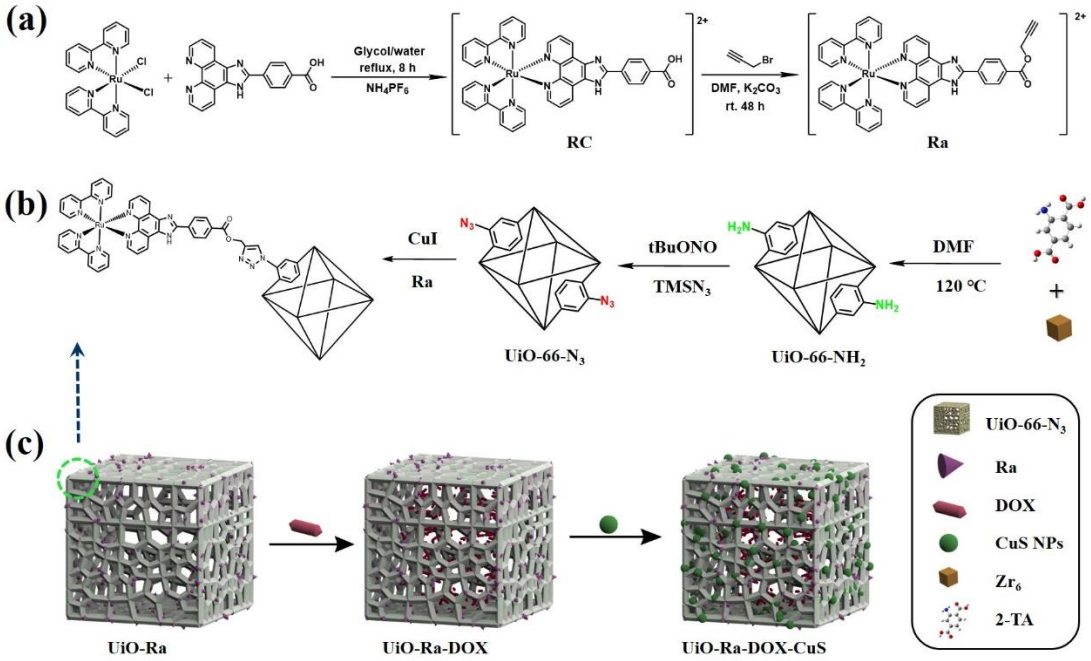

Scheme 1. Schematic illustration of (a) the synthesis of Ra and (b) preparation of UiO-Ra and (c) UiO-Ra-DOX-CuS.

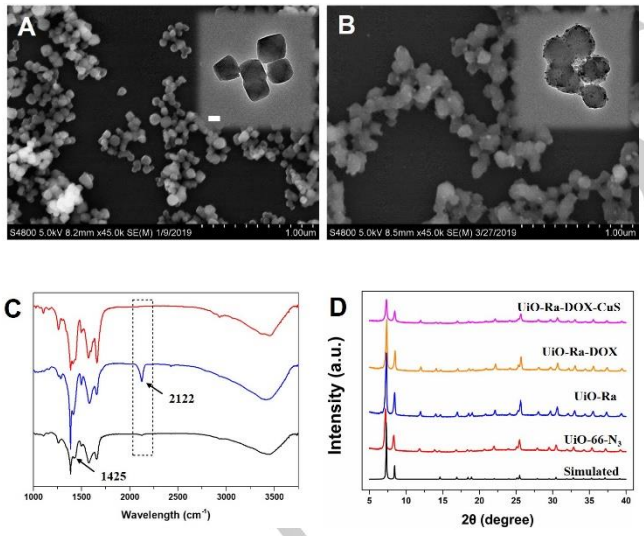

Figure 1. (A) SEM and TEM images (insert) of UiO-66-N_3. (B) SEM and TEM (insert) images of UiO-Ra-DOX-CuS. Scale bar of TEM image is 50 nm. (C) FTIR spectra of UiO-66-NH_2 (red line), UiO-66-N_3 (blue line) and UiO-Ra (black line). (D) XRD patterns of nanoparticles.

A covalent post-synthetic method was adopted to achieve yellow powder of UiO-Ra by a click chemistry reaction. The typical peak of azide groups near 2122 cm^{-1} (asymmetric azide stretching) of UiO-66-N_3 was confirmed by FTIR spectrum (Figure 1C). FTIR spectrum of UiO-Ra showed that the typical absorption peak of azide group nearly disappeared, and the peak at 1425 cm^{-1} of the N=N bond (symmetrical and asymmetrical stretching) obviously appeared, revealing the completion of click reaction and high yield. According to the inductively coupled plasma-optical emission spectrometer (ICP-OES) result (Table S1), the loading capacity of Ra was about 10.2 % for UiO-Ra. Microporous Brunauer-Emmett-Teller (BET) analysis was used to characterize the surface area and porosity of UiO-Ra. The BET surface area of UiO-Ra was calculated to be 857.89 m^2/g with 1.64 nm pore width, which was beneficial to the DOX loading[15] (Figure S3).

After Ra and DOX incorporation, the resulting UiO-Ra and UiO-Ra-DOX showed similar XRD curves compared with UiO-66-N_3 (Figure 1D), demonstrating the maintenance of its crystalline structure after the modification. As shown in Figure S4, CuS NPs were synthesized successfully with an average diameter of approximate 10 nm. After the loading of CuS, SEM and TEM images showed that morphology of MOFs was not been destroyed and CuS NPs were uniformly dispersed on the surface of UiO-Ra-DOX via electrostatic affinity (Figure 1B). In addition, the zeta potential of UiO-Ra-DOX-CuS reduced from 5.6 mV to -2.3 mV (Figure S5) because of the negatively charged CuS NPs loaded onto UiO-Ra-DOX, illustrated the successful modification of the nanoparticles.

After the functionalization of UiO-Ra with DOX, the characteristic DOX absorption peak at 498 nm shifted to 510 nm on account of

10.1002/chem.201904704

DOX hydrophobicity transformation[16] (Figure 2A). The loading capacity of DOX in nanoplatform was estimated to be 13.5 wt.% by UV-Vis spectroscopy measurement at 480 nm (Figure S6A-C), meanwhile, an obvious fluorescence quenching of DOX occurred as a result of the strong interaction between DOX and MOFs[15b] (Figure S6D). Compared with UiO-Ra-DOX, UiO-Ra-DOX-CuS showed remarkable enhanced photoabsorption as wavelength increases from 700 to 1000 nm (Figure 2A), which would be beneficial to photothermal heating under NIR laser irradiation. And the loading capacity of CuS NPs was about 6.8 wt.% for UiO-Ra-DOX-CuS by IPC-OES measurement. Elemental mapping images (Figure 2B) revealed the expected elements dispersed uniformly, further confirming the successful preparation of UiO-Ra-DOX-CuS.

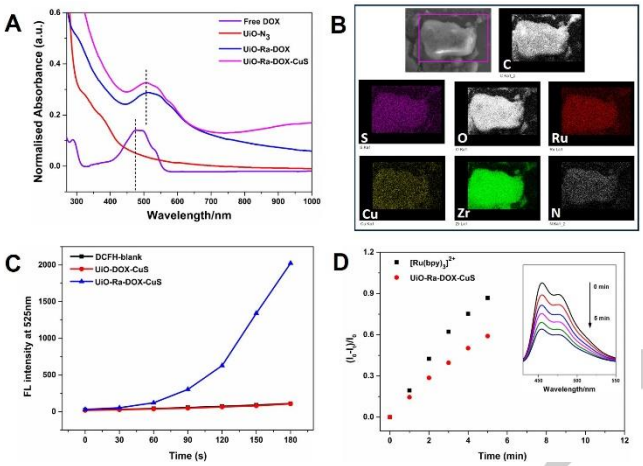

Figure 2. (A) UV-Vis-NIR absorption spectra of different nanoparticles and free DOX. (B) SEM-elemental mapping of UiO-Ra-DOX-CuS. (C) Comparison of the average increase rate of DCFH in the presence of different NPs at 30 s intervals under 450 nm LED irradiation (15 mW/cm^2). (D) The reduction of the fluorescence intensity of DPBF versus time. Inset: emission spectra of mixture of UiO-Ra-DOX-CuS and DPBF upon irradiation.

$^1O_2$ is considered to be the main cytotoxic species in PDT. The $^1O_2$ generation of UiO-Ra-DOX-CuS was evaluated using single oxygen sensor green (DCFH), which could emit strong fluorescence at 525 nm after reacting with $^1O_2$. The mixture of UiO-DOX-CuS and indicator emitted a weak increase of fluorescence under 450 nm irradiation, which meant UiO-DOX-CuS showed a relatively low photoactivity (Figure 2C and S7A). While in the presence of UiO-Ra-DOX-CuS under continue illumination, the fluorescence intensity was significant enhanced, which indicated that UiO-Ra-DOX-CuS can generate $^1O_2$ efficiently upon excitation at 450 nm.

The geometric structure of Ra-terephthalic acid (Ra-TA) was obtained by Density Functional Theory (DFT) computation (Figure S8A),[17] and the contours of the frontier orbitals of Ra-TA are shown in Figure S8B. The energy of first excited triplet states (T1) of Ra-TA lies above 0.98 eV greater than the energetic limit required for yielding $^1O_2$.[18] Simultaneously, the $^1O_2$ quantum yield of UiO-Ra-DOX-CuS was determined to be 0.54 by choosing DPBF as $^1O_2$ indicator, using $[Ru(bpy)_3]^{2+}$ as the standard, whose $^1O_2$ quantum yield was 0.81 in methanol[9c] (Figure 2D).

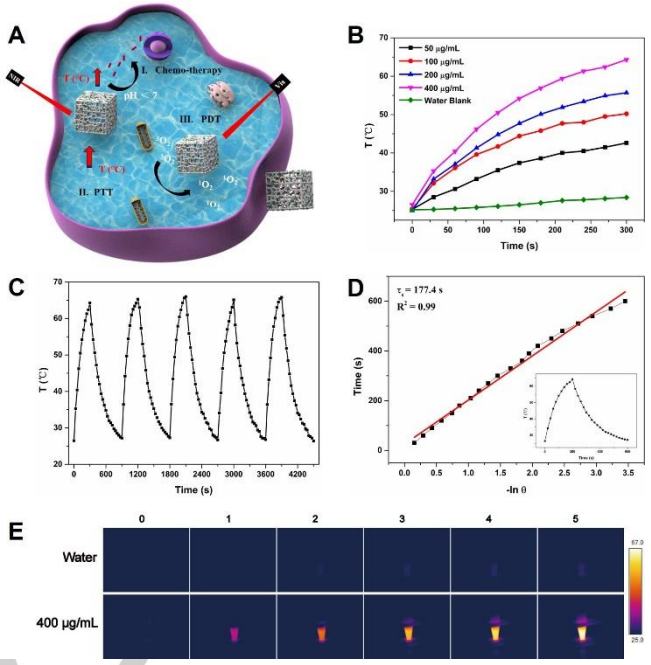

Figure 3. (A) Schematic illustration of UiO-Ra-DOX-CuS based combination of CT, PTT and PDT. (B) Temperature elevation of UiO-Ra-DOX-CuS with different concentrations under 808 nm laser irradiation for 300 s. (C) Temperature variation of UiO-Ra-DOX-CuS dispersion (400 μg/mL) with 808 nm laser (1.5 W/cm^2) on and off for five cycles. (D) Plot of cooling time date *vs* –lnθ. Inset: the photothermal effect of an aqueous dispersion of UiO-Ra-DOX-CuS under 808 nm laser irradiation for 300 s. (E) The infrared temperature (IRT) images of UiO-Ra-DOX-CuS (400 μg/mL) compared with water blank.

Subsequently, it is expected that UiO-Ra-DOX-CuS has a great potential as an excellent photothermal agent as a result of the obvious NIR adsorption of UiO-Ra-DOX-CuS. To overcome the hyperthermia effects of adjacent tissue induced by water, 808 nm was chosen for photothermal measurement based on the minimized absorption of water. As shown in Figure 3, the temperature of NPs dispersions could be elevated under the irradiation obviously. When the concentration of NPs gradually increased from 50 to 400 μg/mL, the corresponding temperature elevation (ΔT) after 5 min irradiation was ≈15.7, 23.9, 33.4 and 46.1 °C, respectively (Figure 3B), indicating the photothermal effect highly depended on the concentration of NPs. As a control, the temperature of UiO-66-N_3 dispersion (Figure S9) or pure deionized water just showed negligible increase under the same irradiation conditions, which revealed that free MOFs and laser irradiation alone would cause minimal thermal effect. Finally, the photothermal stability of NPs dispersion to respond to photoexcitation was examined. As presented in Figure 3C, five cycles of laser on/off with 808 nm laser were recorded. The consistent limit temperature was observed, indicating remarkable photothermal stability of UiO-Ra-DOX-CuS NPs. Meanwhile, the strong photothermal effect also provided a high IR thermal (IRT) imaging property (Figure 3E). In addition, the photothermal conversion efficiency of NPs was calculated to be 26.8 % (Figure 3D) according to reference method[19] .

10.1002/chem.201904704

DOX release behavior of UiO-Ra-DOX-CuS was investigated in PBS at different pH (5.0 and 7.4). The pseudo intercellular cancer cell medium (pH 5.0) can induce faster DOX release rate than the physiological pH medium (pH 7.4). About 48.5% DOX released from UiO-Ra-DOX-CuS after 24h at pH 5.0, which is much higher than that at pH=7.4 (~30.5%) at the same interval (Figure 4A). The pH-responsive DOX release is likely due to the increased protonation of DOX molecules and weakened interactions between MOFs and DOX.[15b] In addition, an enhanced DOX release was observed upon laser irradiation (Figure 4B), indicating the laser-responsive drug release, and the behavior of promotional drug release could be attributed to the photothermal effect of UiO-Ra-DOX-CuS, which would intensify thermal vibration and facilitate DOX dissolution from NPs.[16] Time-dependent cellular uptake of UiO-Ra-DOX-CuS NPs was carried out by ICP-OES upon the digested cell solutions. Figure S10 showed an increasing weight amount of Zr entering into the cells under different incubation time. The result could indicate that UiO-Ra-DOX-CuS NPs managed to be internalized into MDA-MB-231 cancer cells through endocytosis.[9a]

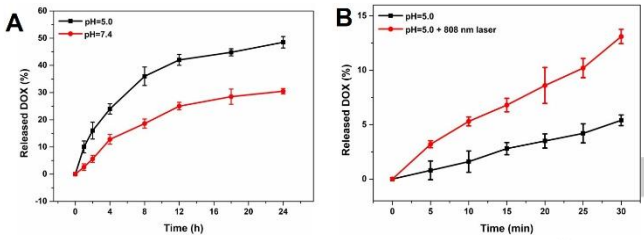

Figure 4. (A) The release profile of DOX at pH=7.4 and 5.0 within 24 h. (B) DOX release profile in PBS buffer (pH=5.0) in the absence and presence of 808 nm laser irradiation.

Additionally, ROS are the most important mediators of cell death induced by PDT. We move to test the ROS production ability of UiO-Ra-CuS in living MDA-MB-231 cells by using DCFH-DA as the indicator. As illustrated in Figure 5, for irradiation alone or UiO-Ra-CuS under dark group, negligible fluorescence was observed. However, increased $^1O_2$ production was visualized after 450 nm LED irradiation (15 mW/cm^2, 10 min) with UiO-Ra-CuS, as indicated through the higher green fluorescence emission of DCFH. As a result, UiO-Ra-CuS can efficiently produce ROS in MDA-MB-231 cells upon PDT.

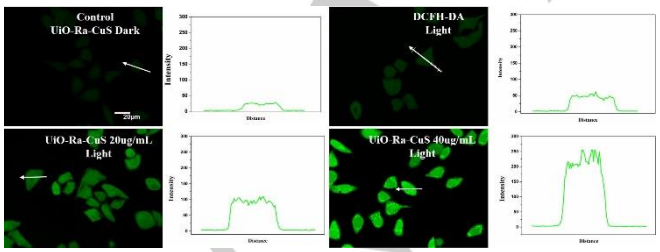

Figure 5. Confocal microscopic images (left) and fluorescent intensity (right) of cellar ROS levels detected by DCFH-DA staining. MDA-MB-231 cells were incubated with UiO-Ra-CuS at the indicated concentrations and irradiation with 450 nm LED (15 mW/cm^2, 10 min). Scale bar: 20 μm.

MTT assay was employed to measure the cell viability of MDA-MB-231 cells after incubating with UiO-Ra-CuS or UiO-Ra-DOX-CuS. Without irradiation, the cells viability nearly did not decrease for the group with drug-free UiO-Ra-CuS, indicating that UiO-Ra-CuS possess good biocompatibility. With the same concentration of Ra under 450 nm irradiation, UiO-Ra-CuS could more efficiently induce MDA-MB-231 cells death (Figure S11A). The phenomena may be caused by the increased ruthenium complex cellular uptake of UiO-Ra-CuS compared with free Ra.[20] At 32 μg/mL, 59% of cells, incubated with UiO-Ra-CuS under 450 nm LED irradiation, were killed, and 35% of cells were killed when the cells were treated with UiO-Ra-CuS under 808 nm laser irradiation, which reveals that UiO-Ra-CuS NPs possess highly efficient antitumor therapy by PDT and PTT (Figure 6A). Consistently, the cell viability decreased with the increased concentration of UiO-Ra-DOX-CuS, suggesting the efficient chemotherapy efficacy (Figure 6B). And the inhibitory efficacy of UiO-Ra-DOX-CuS under dark was little weaker than free DOX at equivalent concentration (Figure S11B). Next, the synergistic therapy of UiO-Ra-DOX-CuS was explored. MDA-MB-231 cells were treated by UiO-Ra-DOX-CuS under dark (CT), UiO-Ra-DOX-CuS + LED (CT-PDT), UiO-Ra-DOX-CuS + laser (CT-PTT) and UiO-Ra-DOX-CuS + LED + laser (CT-PDT-PTT) for the cell viability measurement. Under NIR irradiation, UiO-Ra-CuS could hardly kill the cells at the concentration of 16 μg/mL because the hyperthermia is relatively deficient in this case, but as shown in Figure 6B, CT-PTT group revealed stronger destroying efficacy than chemotherapy alone (69% *vs.* 42%). This may be due to two reasons. First, the progress of drug release could be promoted by local hyperthermia. Meanwhile, the local hyperthermia may enhance the cell metabolism and then increase the drug uptake.[21] Obviously, the highest cell lethality appeared in the group of CT-PDT-PTT. The above results definitely demonstrated the efficient synergistic therapy by the combination of CT, PDT and PTT.

In addition, the above antitumor activities of NPs with or without irradiation were investigated by fluorescence images of live/dead co-staining. The cells can be differentiated to live (green) and dead (red) cells by staining calcein acetoxymethyl ester (Calcein AM) and propidium iodide (PI). No toxicity was observed for irradiation alone (Figure 6C). In contrast, after the irradiation, the cell viability decreased distinctly. When CT, PDT and PTT treatments were combined, nearly 100% of cells were destroyed, where the NIR irradiation not only promote the NPs to produce hyperthermia but also trigger the release and diffusion of DOX. These results reveal that multimodal synergistic treatment would enhance anti-cancer effect and reduce dose of the therapeutic agents, which was consistent with the results of toxicity.

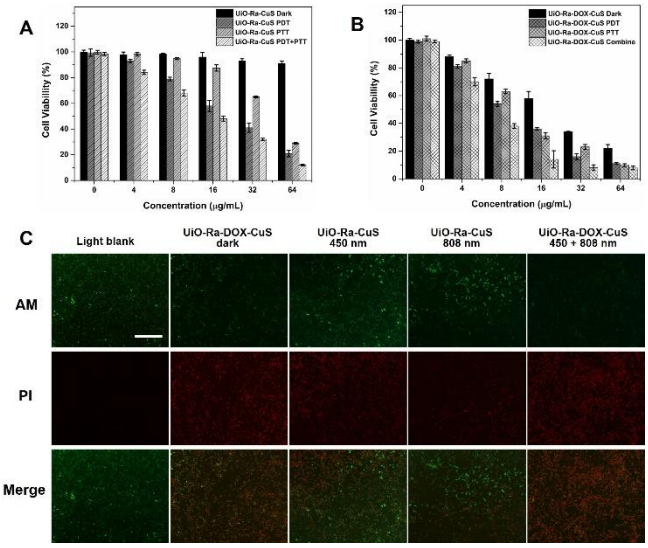

Figure 6. (A)(B) Cell viability of MDA-MB-231 cells after various treatment via MTT assay. (C) Calcein-AM (green, living cells) and PI (red, dead cells) staining analysis of MDA-MB-231 cells incubated with 32 μg/mL UiO-Ra-DOX-CuS, UiO-Ra-CuS + 450 nm (15 mW/cm^2, 30 min), UiO-Ra-CuS + 808 nm (1.5 W/cm^2, 10 min) and UiO-Ra-DOX-CuS + 450 nm + 808 nm. Scale bar: 100 μm.

Conclusions

In conclusion, we have reported the synthesis and synergetic treatment of the Ru(II) polypyridyl complex based NPs with great potential in multi-modal therapy. The synthesis route gave a new way to modify the MOFs with Ru(II) polypyridyl complexes, in which the inherent functionalities are integrated. The small CuS takes PTT function to nanoplatform, and DOX molecules were loaded in the porous of MOFs to realize the multi-modal therapy with chemotherapy function. More attractively, DOX can be promoted to release under acid condition or NIR irradiation. The cell experiments demonstrate that the synergetic treatment of UiO-Ra-DOX-CuS can kill cancer cells effectively and is more efficient than mono therapy (PDT or PTT or CT). Overall, such a simple but powerful multifunctional theranostic platform is promising to explore the potential application in the cancer therapy.

Experimental Section

Materials. Zirconium chloride ($ZrCl_4$), 2-Aminoterephthalic acid (NH_2-BDC), dimethylformamide (DMF), tert-butyl nitrite (tBuONO), azidotrimethylsilane ($TMSN_3$), CuI, N, N-diisopropylethylamine (DIPEA), THF and ethanol were purchased from Adamas. Copper (II) chloride dihydrate ($CuCl_2 \cdot 2H_2O$), sodium sulfide nonahydrate ($Na_2S \cdot 9H_2O$) and polyvinylpyrrolidone (PVP-k30, Molecular weight of 40 KDa) were purchased from Aldrich. Fetal bovine serum (FBS), phosphate-buffered saline (PBS), Dulbecco's modified Eagle medium (DMEM), penicillin streptomycin solution, and trypsin were ordered from KaiJi (Nanjing, China). Unless otherwise noted, all chemicals were used without further purification.

Characterizations. Scanning electron microscopy (SEM) was carried out on a Hitachi S-4800 scanning electron microscope. Transmission electron microscopic (TEM) images were obtained with a TEOL JEM-2100 transmission electron microscope. Powder X-ray diffraction was recorded with a Bruker D8 VENTURE X-ray diffractometer with Cu Kα radiation source. Zeta-potential measurements were conducted on a Malvern Zetasizer Nano ZS instrument. Emission spectra were measured on a Hitachi F-7000 spectrofluorophotometer. Confocal fluorescence imaging was performed on a laser confocal scanning microscope (FluoView FV-1000). Loading capacity of Ra were determined by the inductively coupled plasma (ICP) spectra spectrometry (PE 8300). The surface area and pore size of the synthesized MOFs was determined by microporous BET surface area analyzer (Quantachrome Instruments). Singlet oxygen generation, PDT experiments were carried out with 450 nm LED lamp. The 808 nm NIR laser (Changchun Laser) were used to carry out the PTT study. The camera (DALI TECHNOLOGY) was utilized to monitor the photothermal conversion.

Preparation of Ru(II) polypyridyl alkyne complex (Ra)

Ra was synthesized and characterized as our previous work.[14] ^{1}H NMR (400 MHz, DMSO) δ 9.09 (d, J = 7.5 Hz, 2H), 8.90 (d, J = 8.4 Hz, 2H), 8.86 (d, J = 8.2 Hz, 2H), 8.50 (d, J = 8.6 Hz, 2H), 8.23 (ddd, J = 8.0, 4.4, 1.4 Hz, 4H), 8.12 (td, J = 8.0, 1.4 Hz, 2H), 8.03 (d, J = 4.7 Hz, 2H), 7.91 (dd, J = 8.2, 5.3 Hz, 2H), 7.86 (d, J = 4.9 Hz, 2H), 7.60 (ddd, J = 7.2, 5.8, 3.1 Hz, 4H), 7.39 – 7.34 (m, 2H), 5.03 (d, J = 2.4 Hz, 2H), 3.69 (t, J = 2.4 Hz, 1H). ^{13}C NMR (151 MHz, DMSO) δ 171.89, 165.13, 157.26, 157.05, 151.87, 151.85, 145.45, 138.38, 138.23, 130.86, 130.62, 128.34, 128.21, 127.13, 126.61, 124.91, 124.83, 78.88, 78.61, 53.16.

Preparation of UiO-66-N_3.

UiO-66-NH_2 was synthesized by modified solvothermal method according to the reference.[22] An amount of 9 mL of DMF containing zircomiun tetrachloride (116.6 mg, 0.5 mmol), 2-aminoterephthalic acid (2-TA) (85.1 mg, 0.47 mmol), benzoic acid (0.92 g, 7.6 mmol) and hydrochloric acid (83 μL) were heated at 120 ℃ for 48 h. After cooling, the resulting product was washed with DMF and ethanol for several times, collected through centrifugation (12000 rpm × 10 min) and dried under vacuum. The dried UiO-66-NH_2 (20 mg) were placed in a flask that included 5 mL of THF. Then, 187.5 μL of the tert-butyl nitrite (tBuONO) and 175 μL of the azidotrimethylsilane ($TMSN_3$) were added. The mixture was incubated at the room temperature overnight to produce the azide intermediate corresponding compound (UiO-66-N_3).

Preparation of UiO-66-N_3-Ra (UiO-Ra).

A slurry of UiO-66-N_3 (10 mg), 500 μL Ra (10 mg/mL, DMSO), CuI (1.9 mg) and N, N-diisopropylethylamine (12.9 mg) in 5 mL THF was stirred at room temperature overnight. And the sample was purified and collected by centrifugation (12000 rmp, 10 min) followed by solvent exchange (3 x DMF and 3 x ethyl alcohol), then the sample was dried under vacuum.

Preparation of UiO-Ra-DOX .

To evaluate the drug loading and releasing properties, DOX was employed as a model. Typically, UiO-Ra dispersion (0.5 mg/mL in PBS, pH=7.4) was mixed with DOX solution (0.25 mg/mL), the mixture was placed on the shaker at room temperature for 24 h under dark conditions. The DOX loaded UiO-Ra were collected by centrifugation and washed with PBS several times until the supernatant solution do not have signal of DOX. The concentration of the supernatant was measured by UV-vis spectroscopy at 480 nm. The DOX loading capacity (LC) was calculated as follows:

LC (wt%) = (weight of loaded DOX / total weight of loaded DOX and UiO-Ra) × 100%.

Synthesis of PVP-modified CuS NPs.

According to the reported literature[8a] with slight modification, CuS NPs were prepared successfully. Typically, the mixture of 5 mL of PVP solution (8 mg/mL) and 35 mL $CuCl_2$ solution (0.2 mg/mL) were stirred for 30 min at room temperature. Next, under stirring, 160 μL of freshly-prepared Na_2S aqueous solution (60.54 mg/mL) was added into the above mixture. After 5 min, the mixture was kept in a 90 °C oil-bath for another 20 min. The resulting product was stored under 4 °C for further using and testing.

Preparation of UiO-Ra-DOX-CuS.

5 mg UiO-Ra-DOX was added to 10 mL stock solution of CuS, after that the mixture solution was kept for further 1 h under stirring. Then, UiO-Ra-DOX-CuS NPs were collected by centrifugation and washed with water for three times.

DOX release properties.

In vitro DOX release from UiO-Ra-DOX-CuS NPs was studied as reported method.[23] Briefly, for the pH-responsive DOX release study, drug-loaded NPs (5 mg) were placed in centrifuge tubes and redispersed in PBS solutions with pH values 5.0 and 7.4, respectively (5 mL). And then, the tubes were shaken under dark at 37 °C. After different time intervals (1, 2, 4, 8, 12, 18 and 24 h), the supernatant was collected by centrifugation and transferred into another tube for UV-vis spectroscopy analysis. 5 mL fresh PBS (pH= 5.0 or 7.4) was added into the tubes to redisperse the precipitations, and the tubes were shaken again for the next measurement. For the NIR-triggered DOX release study, UiO-Ra-DOX-CuS dispersion (1 mg/mL, 2.0 mL in PBS, pH=5.0) was irradiated under 808 nm (1.5 W/cm^2) for 30 min, and the release DOX at determinate time point was measured by UV-vis spectrum as the method above.

Cell culture.

MDA-MB-231 cells were cultured in high glucose DMEM supplemented with 10% fetal calf serum and 1% penicillin-streptomycin solution (10 000 U/mL) at 37 °C with incubator 5% CO_2.

Cellular uptake.

Cellular uptake behaviors of UiO-Ra-DOX-CuS in MDA-MB-231 cells were studied by ICP-OES. MDA-MB-231 cells were incubated with UiO-Ra-DOX-CuS 25 μg/mL for 2, 4 and 8 h, and then washed with PBS and digested by trypsine-EDTA. The cells were collected by centrifugation. The precipitations were boiled with 10 mL aqua regia and the solutions were diluted 10 times with ultrapure water. All of the groups contain three independent samples, respectively.

***In vitro* singlet oxygen generation.**

In vitro single oxygen generation measurement was carried out using 2',7'-dichlorofluorescein (DCFH) as capture agent. An amount of 1 mL of PBS buffer (pH=7.4) containing 10 μL of DCFH (2 mM) and 10 μL of photosensitizer samples (2 mg/mL) in a quartz cuvette was illuminated under a 450 nm LED power (15 mW/cm^2) at room temperature for 180 s. The fluorescence intensity of DCFH was recorded at 30 s intervals. The rate of singlet oxygen generation was determined from the increased fluorescence intensity over time. The quantification of singlet oxygen was obtained by the previous literature reported method. Herein, $[Ru(bpy)_3]^{2+}$ was chose as the standard, and the singlet oxygen formation quantum yield of $[Ru(bpy)_3]^{2+}$ was determined to be 0.81 in air-saturated methanol.[24]

The intracellular ROS under irradiation was measured using the fluorescent probe 2',7'-dichlorofluorescein diacetate (DCFH-DA). MDA-MB-231 cells were seeded into glass-bottomed dish at an initial cell density of 1 × 10^5 cells/well in 1 mL of DMEM medium. After 4 h incubation, the cell culture medium was removed and cells were washed twice with PBS buffer (pH = 7.4) before fixed with fresh media containing 10 μM DCFH-DA for 20 min at room temperature. Assembled glass-bottomed dish was illuminated under a 450 nm LED (15 mW/cm^2) at room temperature for 10 min before observation by confocal laser scanning microscope (FluoView FV-1000). DCFH was excited with 488 nm and the green emission was collected with filter range of 500-550 nm.

***In vitro* photothermal performance.**

The UiO-Ra-DOX-CuS aqueous dispersions (0, 50, 100, 200, 400 μg/mL) in a tube were irradiated by an 808 nm laser (1.5 W/cm^2) for 5 min. The changed temperature was recorded and imaged simultaneously with an infrared thermal imaging camera.

***In vitro* the synergic therapeutic efficacy.**

The *in vitro* cytotoxicity of UiO-Ra-DOX-CuS was evaluated by standard 3-(4,5-dimethylthialzol-2-yl)-2,5-diphenyltetrazolium bromide (MTT) assay against MDA-MB-231 cells. Cells harvested in a logarithmic growth phase were seeded in 96-well plates at a density of 10^4 cells/well and incubated overnight and then were treated with UiO-Ra-CuS or UiO-Ra-DOX-CuS at different concentrations (0, 4, 8, 61, 32 and 64 μg/mL) for 4 h. For PDT and PTT groups, MDA-MB-231 cells were irradiated under 450 nm (15 mW/cm^2) LED for 30 min and 808 nm (1.5 W/cm^2) laser for 10 min, respectively. PDT + PTT group was conducted under 808 nm irradiation for 10 min firstly and then 450 nm for 30 min. For imaging, MDA-MB-231 cells was stained by Calcein AM and PI (Beyotime kit) and then imaged using a fluorescence microscope.

Acknowledgements

This work was supported by the National Nature Science Foundation of China (21877084, 21671150, 81171646, 31170776, 21472139), the Science and Technology Commission of Shanghai Municipality (14DZ2261100), as well as by the Fundamental Research Funds for the Central Universities (kx0150720173382).

Keywords: click reaction • drug delivery • nanoplatform • Ru(II) polypyridyl complex • multimodal cancer treatment

[1] H. Wang, B. Lv, Z. Tang, M. Zhang, W. Ge, Y. Liu, X. He, K. Zhao, X. Zheng, M. He, W. Bu, *Nano Lett.* **2018**, *18*, 5768-5774.

[2] a) Y. Wang, X. Liu, G. Deng, J. Sun, H. Yuan, Q. Li, Q. Wang, J. Lu, *Nanoscale* **2018**, *10*, 2866-2875; b) G. Lan, K. Ni, W. Lin, *Coordin. Chem. Rev.* **2019**, *379*, 65-81.

[3] T. Zhao, L. Chen, Q. Li, X. Li, *J. Mater. Chem. B* **2018**, *6*, 7112-7121

[4] D. Zhang, Y. Zheng, C. Tan, J. Sun, W. Zhang, L. Ji, Z. Mao, *ACS Appl. Mater. Inter.* **2017**, *9*, 6761-6771.

[5] Y. Liu, W. Zhen, L. Jin, S. Zhang, G. Sun, T. Zhang, X. Xu, S. Song, Y. Wang, J. Liu, H. Zhang, *ACS Nano* **2018**, *12*, 4886-4893.

[6] a) D. Zhang, Y. Zheng, H. Zhang, J. Sun, C. Tan, L. He, W. Zhang, L. Ji, Z. Mao, *Adv. Sci.* **2018**, *5*, 1800581; b) X. Wang, J. Zeng, M. Zhang, X. Zeng, X. Zhang, *Adv. Funct. Mater.* **2018**, *28*, 1801783.

[7] a) J. Zhou, Y. Jiang, S. Hou, P. K. Upputuri, D. Wu, J. Li, P. Wang, X. Zhen, M. Pramanik, K. Pu, H. Duan, *ACS Nano* **2018**, *12*, 2643-2651; b) T. Zhang, C. Xu, W. Zhao, Y. Gu, X. Li, J. Xu, H. Chen, *Chem. Sci.* **2018**, *9*, 6749-6757; c) C. Bi, J. Chen, Y. Chen, Y. Song, A. Li, S. Li, Z. Mao, C. Gao, D. Wang, H. Möhwald, H. Xia, *Chem. Mater.* **2018**, *30*, 2709-2718.

[8] a) Z. Wang, X. Tang, X. Wang, D. Yang, C. Yang, Y. Lou, J. Chen, N. He, *Chem. Commun.* **2016**, *52*, 12210-12213; b) X. Sun, J. Sun, B. Dong, G. Huang, L. Zhang, W. Zhou, J. Lv, X. Zhang, M. Liu, L. Xu, X. Bai, W. Xu, Y. Yang, X. Song, H. Song, *Biomaterials* **2019**, *201*, 42-52; c) L. Chen, L. Zhou, C. Wang, Y. Han, Y. Lu, J. Liu, X. Hu, T. Yao, Y. Lin, S. Liang, S. Shi, C. Dong, *Adv. Mater.* **2019**, e1904997.

[9] a) R. Chen, J. Zhang, J. Chelora, Y. Xiong, S. V. Kershaw, K. F. Li, P. K. Lo, K. W. Cheah, A. L. Rogach, J. A. Zapien, C. S. Lee, *ACS Appl. Mater. Inter.* **2017**, *9*, 5699–5708; b) S. Monro, K. L. Colon, H. Yin, J. Roque, III, P. Konda, S. Gujar, R. P. Thummel, L. Lilge, C. G. Cameron, S. A. McFarland, *Chem. Rev.* **2019**, *119*, 797-828; c) J. Liu, Y. Chen, G. Li, P. Zhang, C. Jin, L. Zeng, L. Ji, H. Chao, *Biomaterials* **2015**, *56*, 140-153.

[10] J. Liu, C. Zhang, T. W. Rees, L. Ke, L. Ji, H. Chao, *Coordin. Chem. Rev.* **2018**, *363*, 17-28.

[11] W. Zhang, J. Xiao, Q. Cao, W. Wang, X. Peng, G. Guan, Z. Cui, Y. Zhang, S. Wang, R. Zou, X. Wan, H. Qiu, J. Hu, *Nanoscale* **2018**, *10*, 11430-11440.

[12] W. Chen, X. Yu, A. Cecconello, Y. Sohn, R. Nechushtai, I. Willner, *Chem. Sci.* **2017**, *8*, 5769-5780.

[13] E. Villemin, Y. C. Ong, C. M. Thomas, G. Gasser, *Nat. Rev. Chem.* **2019**, *3*, 261-282.

[14] X. Hu, Z. Xu, J. Hu, C. Dong, Y. Lu, X. Wu, M. Wumaier, T. Yao, S. Shi, *Inorg. Chem. Front.* **2019**, *6*, 2865-2872.

[15] a) A. R. Chowdhuri, D. Laha, S. Chandra, P. Karmakar, S. K. Sahu, *Chemical Engineering Journal* **2017**, *319*, 200-211; b) H. Zhao, Q. Zou, S. Sun, C. Yu, X. Zhang, R. Li, Y. Fu, *Chem. Sci.* **2016**, *7*, 5294-5301.

[16] Z. Li, Y. Hu, Z. Miao, H. Xu, C. Li, Y. Zhao, Z. Li, M. Chang, Z. Ma, Y. Sun, F. Besenbacher, P. Huang, M. Yu, *Nano Lett.* **2018**, *18*, 6778-6788.

[17] S. Shi, X. Gao, H. Huang, J. Zhao, T. Yao, *Chem. Eur. J.* **2015**, *21*, 13390-13400.

[18] A. Galstyan, K. Riehemann, M. Schäfers, A. Faust, *J. Mater. Chem. B* **2016**, *4*, 5683-5691.

[19] Q. Huang, S. Zhang, H. Zhang, Y. Han, H. Liu, F. Ren, Q. Sun, Z. Li, M. Gao, *ACS Nano* **2019**, *13*, 1342-1353.

[20] D. Y. Zhang, Y. Zheng, H. Zhang, L. He, C. P. Tan, J. H. Sun, W. Zhang, X. Peng, Q. Zhan, L. N. Ji, Z. W. Mao, *Nanoscale* **2017**, *9*, 18966-18976.

[21] Z. Li, Y. Hu, T. Jiang, K. A. Howard, Y. Li, X. Fan, Y. Sun, F. Besenbacher, M. Yu, *Part. Part. Syst. Char.* **2016**, *33*, 53-62.

[22] W. Wang, L. Wang, Z. Li, Z. Xie, *Chem. Commun.* **2016**, *52*, 5402-5405.

[23] X. Zeng, W. Tao, L. Mei, L. Huang, C. Tan, S. S. Feng, *Biomaterials* **2013**, *34*, 6058-6067.

[24] A. A. Abdel-Shafi., P. D. Beer., R. J. Mortimer., F. Wilkinson., *J. Phys. Chem. A*, *104*, 192-202.

10.1002/chem.201904704

WILEY-VCH

Entry for the Table of Contents

FULL PAPER

We report here a Ru(II) polypyridyl alkyne complex (Ra) as a photosensitizer which was modified into MOFs by click reaction for the first time. In addition, a new way to integrate chemo-photodynamic-photothermal therapy and dual-stimuli response release into one nanoplatform was presented.

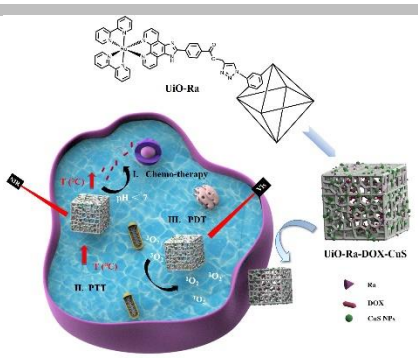

Xiaochun Hu, Yonglin Lu, Chunyan Dong, Wenrong Zhao, Xuewen Wu, Lulu Zhou, Lv Chen, Tianming Yao, Shuo Shi

Page No. – Page No.

A Ru(II) Polypyridyl Alkyne Complex Based Metal–Organic Frameworks for Combined Photodynamic/Photothermal/Chemo-Therapy